Long-Range Carrier Diffusion in (In,Ga)N Quantum Wells and Implications from Fundamentals to Devices

Aurelien David [*]
Google, 1600 Amphitheater Parkway, Mountain View, California 94043, USA

(Received 4 January 2021; revised 14 February 2021; accepted 31 March 2021; published 10 May 2021)

Photoluminescence measurements on high-quality (In, Ga)N quantum wells reveal that carriers diffuse laterally to long distances at room temperature, up to tens of microns. This behavior, which shows a pronounced dependence on the excitation density, contrasts with the common expectation of a short diffusion length. The data is well explained by a diffusion model taking into account the full carrier recombination dynamics, obtained from time-resolved measurements. These observations have important implications for understanding the high efficiency of III-nitride emitters, but also for proper interpretation of photoluminescence experiments and for the design of efficient small-scale devices.

DOI: 10.1103/PhysRevApplied.15.054015

I. INTRODUCTION

Carrier transport in (In, Ga)N compounds has attracted interest due to the complex physics at play. The energy fluctuations stemming from the distribution of In and Ga atoms can localize carriers on the scale of a few nanometers. This influences the macroscopic transport properties, including lateral transport in the plane of thin (In, Ga)N layers, leading to a nontrivial diffusion coefficient that various groups have studied. Some key experimental techniques are near-field microscopy, [1] time-of-flight measurements [2,3], and transient grating spectroscopy [4,5]. Notably, these studies often assume a fast recombination lifetime—a few nanoseconds—in their analysis, translating into a diffusion length (L_d) of a few hundred nanometers. This may appear reasonable for light-emitting diodes (LEDs) in operating conditions. However, as this paper shows, this overlooks the intricacies of (In, Ga)N carrier dynamics.

In this paper, we directly observe long-range lateral carrier diffusion in (In, Ga)N quantum wells (QWs) at room temperature, through simple photoluminescence (PL) experiments. The diffusion length is power dependent, reaching tens of microns at low power. These data are very well explained when the carrier dynamics are considered. We discuss the fundamental and applied consequences of such long-scale diffusion.

II. OBSERVATION OF LONG-RANGE DIFFUSION

The studied samples, provided by Soraa, Inc., are single-QW (In, Ga)N structures embedded in p-i-n junctions specially designed for PL studies. They are grown by metal-organic chemical-vapor deposition on bulk GaN substrates. They have high internal quantum efficiency (IQE). The recombination physics of similar samples have been extensively reported in our previous work [6–9]. The samples are covered with antireflective SiO_2 coatings to avoid reflection of the exciting laser and emitted light.

The PL setup is shown in Fig. 1(a). The beam of a 405-nm laser diode is expanded and focused to a Gaussian spot with a waist of 2.5 μm. The drive current of the laser is varied to control the excitation density [this does not affect the shape of the laser spot, as shown in Fig. 2(a)]. The resulting PL signal is collected by a calibrated spectrometer, which gives access to the absolute PL IQE. Due to the Gaussian spot profile of the laser, the excitation density varies spatially; for simplicity, we define a *nominal* photoexcited current density (J) in a uniform excitation disk, the diameter of which is the beam waist. The laser signal can also be time modulated and the resulting time-dependent PL collected by a network analyzer to determine the differential carrier lifetime, as described in Ref. [6].

A charge-coupled-device (CCD) camera is placed in line with the optical axis to image the laser or PL spot. Laser or PL imaging is selected by inserting appropriate dichroic filters; the image is carefully refocused in each case. A small aperture (diameter approximately 2 mm) is placed in the collimated path of the image, to limit the angular aperture of the collected signal to near-normal incidence.

Figures 1(b) and 1(c) show images of PL spots collected on a sample (4-nm-thick QW, composition [In] = 13%, peak IQE 80%) at two current densities. At moderate density (near peak IQE), the spot extends far away from the laser excitation: the radius where the PL reaches 10% of its peak value (the so-called 10% radius) is more

[*]aureliendavid@google.com

 © 2021 American Physical Society

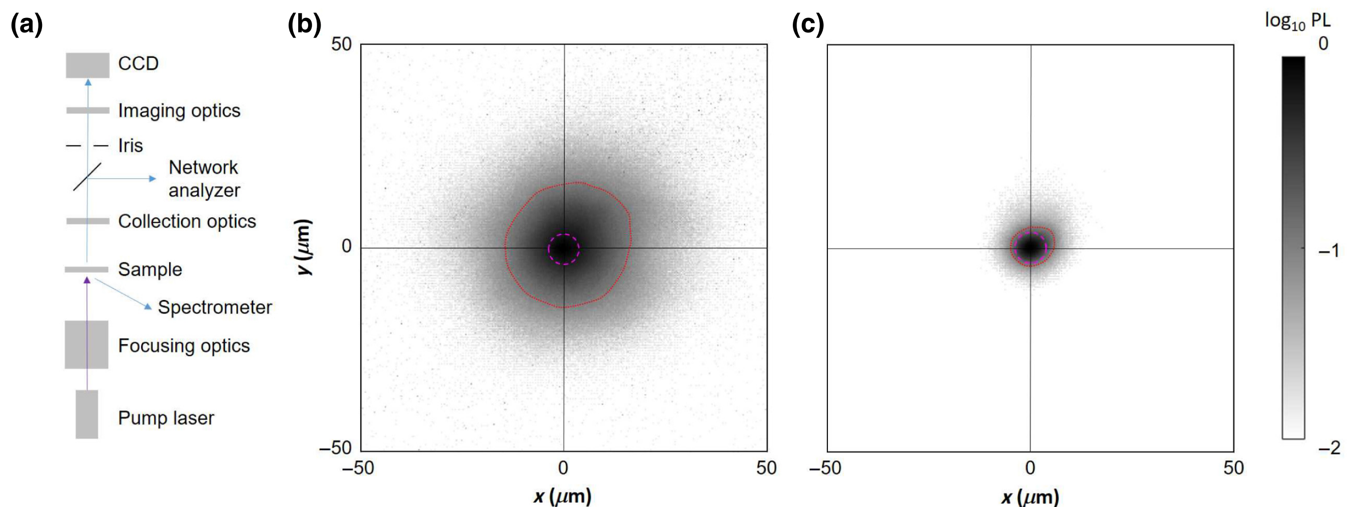

FIG. 1. Photoluminescence experiments. (a) The experimental setup. (b),(c) CCD images of the PL spot (logarithmic scale, shown on the right) at nominal current densities of 25 and 9500 A/cm^2, respectively. The dotted line is the isoline at 10% of the PL intensity. The dashed line is the isoline at 10% of the laser-excitation intensity.

than 10 μm. For comparison, the 10% radius of the laser spot, also shown, is about 3 μm. Note that since luminescence scales with the square of the excitation at low density [in the Shockley-Read-Hall (SRH) regime], the PL spot should actually be *narrower* than the laser spot in the absence of diffusion. At a high excitation density (nominally 10 kA/cm^2), the PL spot is substantially smaller.

These observations are more easily quantified on cross-section plots, shown in Fig. 2(a), at various excitation densities (spanning from peak IQE to the droop regime). The PL spot shape depends strongly on the pump power and extends over tens of micrometers at low power. Given the bimolecular nature of radiative recombination, the underlying carrier density extends even further. The pronounced dependence on the excitation power confirms that optical artifacts cannot account for the large spot size at low excitation. More details are given in the Appendix, where we consider such artifacts in detail (including laser reflection, variations in laser-spot size, PL reabsorption, multiple-bounce signal, and thermal effects) and show they do not influence our measurements.

These data cannot be explained assuming a constant L_d. Instead, a proper interpretation requires consideration of the power-dependent carrier dynamics.

To this effect, joint measurements of the IQE and differential carrier lifetime are performed on the sample at varying power density [6] and fitted by the common *ABC* model to yield recombination coefficients *A* (SRH), *B* (radiative), and *C* (Auger). The *ABC* model is only an approximation, as the radiative and Auger coefficients can display a carrier dependence (as discussed in Refs. [6,10]). Nonetheless, this carrier dependence is modest in the present sample and a standard *ABC* model is suitable. The resulting coefficients are $A = 1.2 \times 10^5$ s^{-1}, $B = 4 \times 10^{-14}$ cm^3 s^{-1}, and $C = 1 \times 10^{-34}$ cm^6 s^{-1}. The very low value of *A* (corresponding to an SRH lifetime of approximately 10 μs) is explained by (1) the high quality of the sample and (2) the thick QW, in which the low electron-hole overlap reduces the SRH coefficient [11].

Armed with this knowledge, the PL data are fitted by a steady-state diffusion model:

$$G = R - D\Delta n, \tag{1a}$$

$$R = An + Bn^2 + Cn^3, \tag{1b}$$

where *R* and *G* are the local recombination and generation rates, *D* is the ambipolar diffusion coefficient (limited by hole diffusion), and *n* is the local carrier density. In Eq. (1a), *R* is commonly written as $R = n/\tau$, with τ (the carrier lifetime) assumed constant. In contrast, in our analysis, *R* depends on the local carrier density—in other words, we take into account the carrier-density dependence of the carrier lifetime $\tau(n)$. This variation is very large: at low density (in the SRH regime), $\tau = 1/A \sim 10$ μs, whereas at high density (in the droop regime), τ reaches a few nanoseconds. This results in a substantial change in the local diffusion length $L_d = \sqrt{D\tau}$, from approximately 50 μm at low density (where $\tau = 1/A$) to less than 1 μm at high density. Note that this model ignores various second-order effects, such as density-induced drift, polarization field screening, and any possible density dependence of *D*.

The model is solved numerically by finite differences with an iterative loop, solving Eqs. (1a) and (1b) in turn until convergence. The spatial distribution of the luminescence is then computed as Bn^2. The data to be fitted

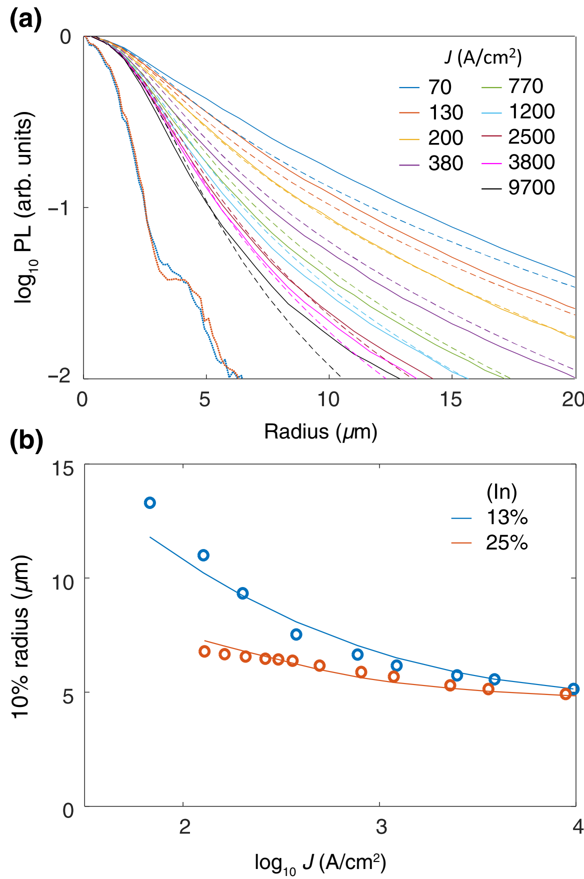

FIG. 2. PL diffusion data. (a) A cross section of the PL versus the radius, for various current densities J: solid lines, experimental data; dashed lines, model; dotted lines, the laser profile at the highest and lowest excitation levels. Note the logarithmic scale. (b) The luminescence spot radius versus the current density, for two samples: circles, experimental data; lines, model.

are the set of PL spot profiles (Fig. 2) and corresponding IQEs at varying power [shown in Fig. 3(b)]. This is a very overspecified data set, since the only free parameter is the diffusion coefficient D. Good fits are obtained for $D = 3$ cm^2 s^{-1}, a value in good agreement with previous reports [1–5]. This confirms that the PL spot size is determined by density-dependent carrier diffusion.

Similar measurements are repeated on a sample with a different QW configuration: thickness 2.5 nm, composition [In] = 25%. Despite its high In composition, this sample has a relatively high peak IQE of 73%. The PL spot size varies with excitation density, albeit in a smaller range than for the previous sample: from 7 μm at low density to 5 μm at high density. Again, these data are well explained by a diffusion model based on lifetime measurements. The experimental and modeled 10% radius are shown in Fig. 2 (b). This sample is best fitted with a higher diffusion coefficient $D = 6$ cm^2 s^{-1}.

Our observations might seem at odds with multiple literature reports of $L_d \sim 100$ nm [4,12,13]. In fact, such a short scale is valid at a high excitation density (associated with a fast lifetime). In contrast, the present measurements, at larger distances and on a logarithmic scale, reveal the long-range behavior. Besides, samples of sufficient quality (i.e., a low A coefficient) are required to observe long-range diffusion—this has not necessarily been the case in past studies.

Nor are our conclusions in conflict with numerous microscopy studies in GaN (e.g., cathodoluminescence) with approximately 100-nm resolution; indeed, GaN has a much faster SRH lifetime (approximately 50 ps [14]) and, accordingly, a short L_d. Regarding microscopy in (In, Ga)N, very few studies exist at room temperature in high-IQE material—both required to observe long-range diffusion. Such a study has been performed in Ref. [15], where it has been found that submicron features become smeared out at $T = 170$ K—in excellent agreement with our findings. Finally, note that the imaging resolution around dislocations is not governed by diffusion [16].

In summary, lateral diffusion in (In, Ga)N QWs can be substantial. Indeed, even in high-carrier-density experiments, the lifetime increases rapidly away from the excited region, leading to a large local L_d. This effect holds true in high-IQE samples, as it goes hand in hand with a slow SRH lifetime, which governs long-scale diffusion. The electron-hole separation, caused by the polarization fields that characterize III-nitride heterostructures, slows down the recombination dynamics overall [9]: this leads to longer L_d than in conventional III–V samples [17] and to the pronounced density dependence reported here.

III. IMPLICATIONS OF LONG-RANGE DIFFUSION

We now discuss three implications of these observations, from fundamental to applied.

A. The IQE of III-nitride quantum wells

A long-standing puzzle is how group-III nitrides can reach a high IQE despite a high threading dislocation density (TDD), as dislocations are believed to act as nonradiative centers. It is often argued that this can be explained by carrier localization at In-rich fluctuations (approximately 10-nm scale), which prevent the carriers from reaching dislocations [18]. However, the long-range diffusion reported here is incompatible with such tight localization. Accordingly, our recent numerical studies have found no support for a fully localized carrier distribution at room temperature but, rather, for a thermalized distribution with a mix of localized and propagative states, as sketched in Fig. 3(a) [8]. Incidentally, the value of D for (In, Ga)N (both here and in other reports) is on the same order as for bulk GaN [19], further confirming that alloy disorder does not lead to full localization.

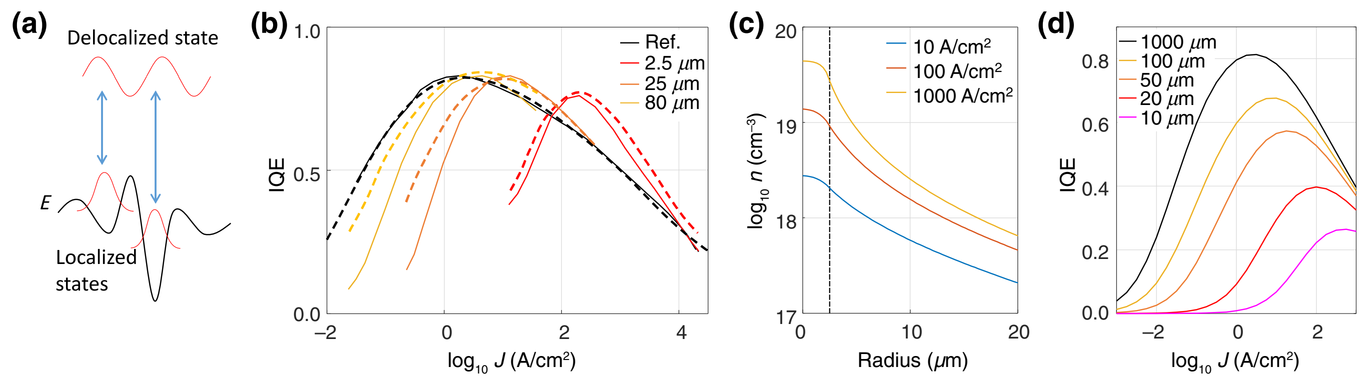

FIG. 3. (a) A sketch of the thermalization process, driven by fast scattering (arrows) between localized and delocalized states (red shapes). (b) The IQE from PL experiments: solid lines, experimental data. The reference curve is obtained by varying the spot size. The other curves, with a constant spot size and varying power, have an altered shape due to diffusion. The dashed lines show the fit by the diffusion model. (c) The modeled diffusion of carriers from an injected area with a 2.5-μm radius (injection boundary shown as dashed line) at various current densities. (d) The modeled IQE of LEDs of varying sizes, with nonradiative side-wall recombinations.

More quantitatively, the present samples are grown on bulk GaN substrates and have a low TDD of approximately $(1-5)\times 10^6$ cm^{-2}. This corresponds to a few dislocations in a 10×10 μm square. It is clear from Fig. 1 that at low-to-moderate excitation density, the carrier distribution will "see" tens of dislocations—yet, this does not preclude a very high peak IQE. This would be even more true in common GaN-on-sapphire samples, where the TDD reaches approximately 10^8 cm^{-2} and a high IQE is nonetheless achievable.

It has also been proposed that delocalization at high density could account for IQE droop [20]. This is also incompatible with our observations, as diffusion actually decreases at higher density. This causes no contradiction with the previously reported trend of a higher contrast at higher current in nanoscopic imaging of (In, Ga)N luminescence [21]: this effect is due to a sharpening of the local carrier distribution (due to lower diffusion) which reveals inherent in-plane inhomogeneities.

Therefore, we conclude that localization alone cannot explain the high IQE of group-III nitrides. Rather, dislocations must have a limited nonradiative effect—possibly due to the shielding effect of local strain [22] or V-shaped pits [23]. In fact, there is conclusive evidence that SRH recombinations are instead mostly caused by point defects [24].

B. Interpretation of PL experiments

The IQE of semiconductors is often studied with power-dependent PL: the excitation is varied to obtain a PL IQE curve without device fabrication. This curve can then be used for temperature-dependent analysis [25] or *ABC* fitting [26].

However, our findings imply that the shape of the IQE curve can be strongly affected by diffusion, especially when a focused laser-spot size is used (which is desirable to reach the droop regime). This is illustrated in Fig. 3(b), which shows the PL IQE curve collected with various laser-spot sizes. In this comparison, the reference IQE curve (the details of which are explained hereafter) is the PL IQE curve associated with the lifetime measurements; it constitutes a "ground truth" for the other PL measurements. In comparison, the measurement with a maximally focused laser spot severely alters the IQE curve: the peak IQE is reached at a much higher nominal current density and the overall shape is much narrower. Qualitatively, it is clear how diffusion causes such distortions: although the laser is tightly focused, the generated carriers diffuse laterally, which results in a much-reduced effective carrier density—thus the late onset of peak IQE and droop. To verify this quantitatively, we compute the IQE versus excitation density, using Eqs. (1a) and (1b). The results, shown in Fig. 3(b), agree very well with the experimental data; they should be compared with the theoretical IQE curve in the absence of diffusion effects, which agrees very well with the reference IQE curve.

As a further confirmation, measurements are repeated with defocused laser spots under two defocus conditions, with diameters 25 and 80 μm, respectively. The resulting IQE curves are shown in Fig. 3(b): as the laser is defocused, the IQE curve shape is modified and progressively converges toward the reference IQE shape. Again, the theoretical IQE curves predicted by the diffusion model are in excellent agreement with measurements.

Clearly, the distortion effects reported here would substantially alter any analysis of the IQE curve and should be minimized. This can be done by using a less-focused laser beam (though this may preclude a high excitation density). A better approach is that used to obtain the reference IQE curve, which we now clarify. This curve is, in fact, obtained by maintaining a constant (maximal) laser power, while progressively defocusing the laser spot

(in contrast to the conventional measurements, where the spot size is constant and the laser power is varied). In this approach, diffusion artifacts are inherently minimized because the excitation spot size increases as the power density decreases: at all but the highest densities, the laser spot is large enough to minimize diffusion artifacts. This advantageous excitation scheme has been used in our previous studies of carrier dynamics [6–9] and is recommended for practitioners of PL measurements.

C. Design of small devices

There is currently much interest in optical devices with small lateral dimensions, including micro-LEDs and lasers [such as narrow-ridge lasers or vertical-cavity surface-emitting lasers (VCSELs)]. In these devices, a small area is injected electrically (e.g., by forming a selective p contact), with the intention of restricting the QW carrier population to the same area. However, our results indicate that carriers will unavoidably diffuse away from the injected area. Figure 3(c) illustrates this. In this calculation, we assume typical recombination coefficients for a thin (approximately 3-nm) blue QW (namely $A = 1.2 \times 10^6\ \text{s}^{-1}$, $B = 3 \times 10^{-12}\ \text{cm}^3\ \text{s}^{-1}$, $C = 1 \times 10^{-31}\ \text{cm}^6\ \text{s}^{-1}$, leading to a peak IQE above 80%) [9,27]. These faster coefficients lead to a shorter L_d than in our first sample—nonetheless, the low-density L_d remains as high as 17 μm: this is directly tied to the moderate value of A characteristic of high-IQE material. We assume a cylindrical injection with a 2.5-μm radius and compute the radial carrier distribution at various current densities. A substantial diffusion is observed, together with a sharpening of the distribution at high density.

For micro-LEDs, this effect has implications regarding nonradiative recombinations at device side walls: it explains how these can affect the efficiency of relatively large devices (even hundreds of micrometers [28])—which would clearly not occur if L_d were only 100 nm. To confirm this, we model the effective IQE of a blue LED (square shape, same recombination coefficients as above) with side-wall recombinations of infinite velocity and varying dimensions. The results, shown in Fig. 3(d), confirm that even for a 100-μm-wide device, side-wall recombinations significantly affect the IQE. This result is in qualitative agreement with experimental data (e.g., Ref. [28]). One could consider adding a noninjected "belt" at the device perimeter to prevent carriers from reaching side-wall defects; even so, however, a sizable long-range diffusion current to the noninjected region is unavoidable and the prospects of this approach are limited. Instead, defect passivation appears more promising [29].

For laser diodes, the diffusing carriers cause a reduction in injection efficiency near threshold, since they cannot contribute to lasing. The quantitative consequences for threshold density and carrier clamping call for future investigations, especially in emerging small-dimension lasers such as VCSELs.

In summary, long-range diffusion must be accounted for in order to understand and optimize micron-scale III-nitride devices.

IV. CONCLUSION

To conclude, we observe carrier diffusion over tens of micrometers in high-quality (In, Ga)N QWs under optical excitation, which stands in contrast to the shorter lengths (approximately 100 nm) often derived by assuming a nanosecond-order carrier lifetime. Our observations are well explained by a conventional diffusion model, with a reasonable diffusion coefficient, if the full carrier dynamics are taken into account. Indeed, the lifetime varies by orders of magnitude with the carrier density, and the diffusion length away from the excited region is governed by the SRH lifetime. Hence, long-range diffusion occurs in high-quality (In, Ga)N materials, due to their slow SRH lifetime. This has several important implications: the high IQE of (In, Ga)N LEDs cannot be simply ascribed to carrier localization; great care must be taken in avoiding diffusion artifacts in photoluminescence experiments; and upcoming small-scale emitters should be designed with long-range diffusion in mind.

APPENDIX: EXCLUSION OF OPTICAL ARTIFACTS

To be certain that the CCD images are actually measuring the PL spot, we investigate and exclude possible optical artifacts, as described below.

1. Laser-spot variations

One may wonder if the profile of the laser spot itself may depend on the laser current. As already shown in Fig. 2, this is not the case: by imaging the laser spot, we find that it remains stable at all currents. As a further confirmation, we repeat experiments where the laser power, rather than being current controlled, is decreased by inserting a density filter in the collimated path of the laser beam (attenuating it 300 times). As shown in Fig. 4, we observe the expected effect: the PL radius increases to 15 μm—the same value as in the main text at the same power density.

Although we discuss other possible artifacts below, we believe that the power dependence of the PL spot, while the laser spot remains the same, is in itself evidence that our observations cannot be caused by an optical artifact (as none would cause such power dependence).

2. Laser reflection

The laser beam is partially reflected on both facets of the sample, which may lead to additional excitation with a

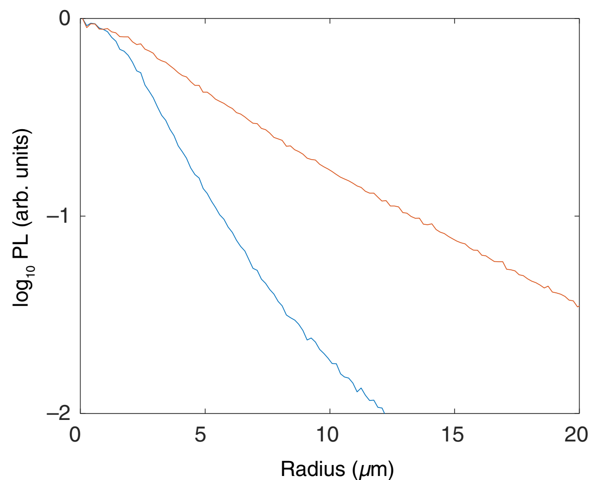

FIG. 4. The PL profile at maximum power (in blue) and with the laser attenuated 300 times by a density filter (in red). The broadening of the PL spot is the same as when the laser power is reduced by controlling the current.

wider spot size. Hereafter, we show that these reflections do not contribute to our observations.

The sample is coated with SiO_2 antireflection layers; the layer on the substrate side is optimized for the laser wavelength (to minimize reflection), with a laser reflection of approximately 1% expected from modeling, and the layer on the epilayer side is optimized for the PL wavelength (to minimize light-extraction effects), with a laser reflection of a few percent expected from modeling.

The actual laser reflection can be measured experimentally in our setup. To this effect, the sample is slightly tilted so that the laser spot after a round trip is offset from the initial laser spot on the CCD image (the offset between the two spots increases with the tilt angle, confirming that the secondary spot is caused by reflections). Note that the focus of the collecting lens of the CCD camera must be slightly adapted to image the laser reflection, due to its extra round trip in the sample. The intensity of the reflection can be measured by the intensity of the imaged spot, as shown in Figs. 5(a) and 5(b): it is about 0.3% of the peak intensity of the laser spot. This is in reasonable agreement with the modeled reflection values (namely, we estimate that the substrate-side reflection is about 3% and the epi-side reflection is about 10%). Given the broadening of the laser spot after reflection (approximately 5 μm radius), the relative peak excitation intensity of the reflected spot is well below 1%, which is too low to induce luminescence on the scale we are observing (our PL data show two decades of dynamic range).

To further confirm unambiguously that this laser reflection does not contribute to the PL measurement, we can actually measure the PL spot size in this tilted-sample geometry. Figures 5(c)–5(e) show such measurements:

(1) Figure 5(c): at the maximum laser power, the initial PL spot has a 10% radius of approximately 4–5 μm. This is the same value as reported in normal-incidence geometry.

(2) Figure 5(d): at this same power, the PL spot size from the laser reflection (which is, of course, offset from the initial PL spot) has a large radius, about 15 μm. This is because the reflected spot is excited at low intensity and hence is much larger due to diffusion. This figure shows an image with a long CCD integration time, such that the primary PL spot is saturated and the reflected PL spot can be measured.

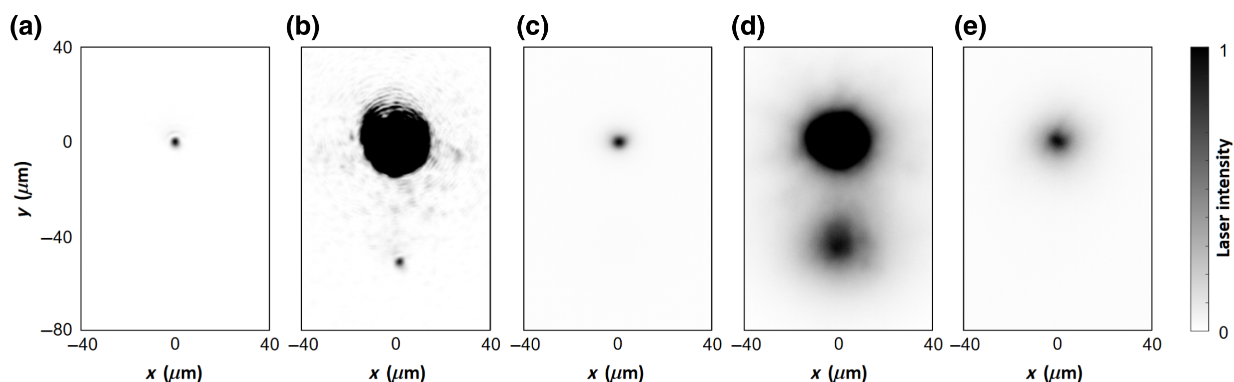

FIG. 5. Images of the laser spot (a),(b) and the PL spot (c)–(e) with a tilted sample. (a) An image of the initial laser spot. (b) The same image with a much longer integration time. The initial spot is saturated and the reflection (after bouncing off the substrate and epilayer interfaces) is visible, with an offset due to the sample tilt. The relative intensity of the reflection is 0.3%. (c) At maximum excitation density, the primary PL spot has a radius of approximately 4–5 μm (the same value as for normal incidence). (d) In the same conditions, but with a much longer integration time, the PL from the reflected laser spot can be seen. It has a large radius, due to the low excitation density and the broadening of the reflected laser spot. The relative peak PL intensity is 1% of the primary PL spot. (e) At lower excitation density, the primary PL spot has a radius of approximately 15 μm (the same value as for normal incidence).

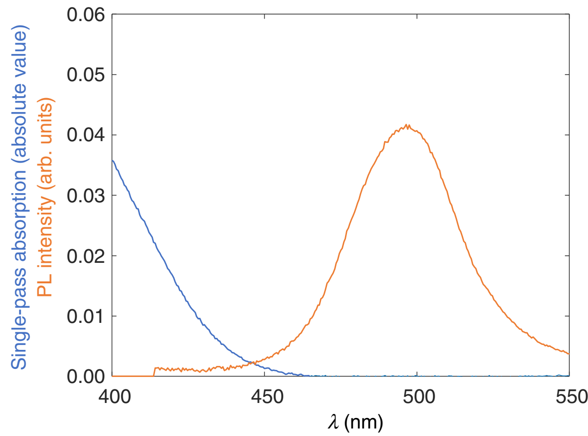

FIG. 6. The PL intensity (at low excitation) and the single-pass absorption of the QW. The strong Stokes shift leads to a low net single-pass reabsorption of approximately 0.02%.

(3) Figure 5(e): at the minimum laser power, the initial PL spot has a 10% radius of 15 μm, again the same as for normal incidence.

In summary, if we tilt the sample to move the laser reflection away from the initial laser spot, we obtain the exact same PL spot sizes as reported previously. This confirms that laser reflection plays no role in the results.

3. PL reabsorption and photon recycling

One may wonder if PL guided inside the sample could be reabsorbed by the QW and lead to PL reemission (a process also known as photon recycling). As we now show, reabsorption in this sample is very weak and causes no contribution to the PL measurements.

The single-pass reabsorption in this single-QW sample is very low. It can be quantified accurately by measuring the absorption and PL spectra, as shown in Fig. 6 (with the PL spectrum shown at low power density).

The corresponding single-pass reabsorption is approximately 0.02%. This very low value is due to having only one QW and to the strong Stokes shift in this sample, caused by the *p*-*i*-*n* geometry. The single-pass reabsorption increases at higher power density (because the PL spectrum blue shifts) and it reaches approximately 0.5% at the highest density investigated.

The resulting net reexcitation of the QW in the experiment is caused by two sources of reflection:

(1) PL reflected from the epilayer surface (located 150 nm away from the QW): this reflection occurs within the same lateral region as the laser spot, because light cannot travel far laterally over such a small thickness.

(2) PL reflected from the substrate surface (located $L = 150$ μm away from the QW): this reflection is diluted by

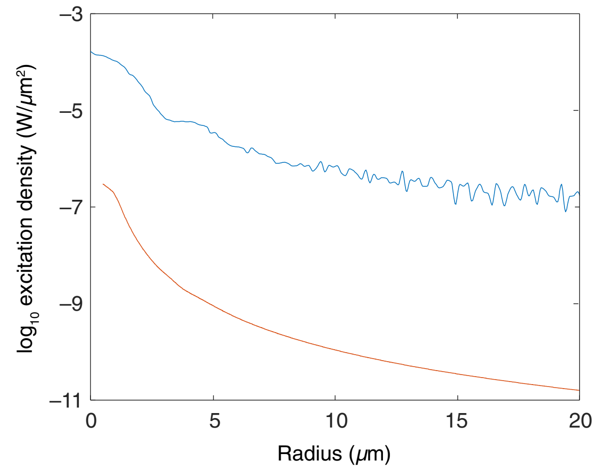

FIG. 7. A comparison of the experimental initial QW excitation by the laser (blue) and the computed reexcitation due to PL reabsorption (red). Reexcitation is always lower by orders of magnitude, precluding any impact on our results. (Note that the long tail of the initial excitation is caused by background noise of the CCD.)

the very long distance traveled and amounts to a very low reexcitation density (scaling with $1/L^2$).

These effects are easily quantified by a simple ray-tracing calculation, taking into account the sample and excitation geometry and the QW reabsorption. The results are shown in Fig. 7. In this calculation, we use the worst-case single-pass absorption of 0.5% (corresponding to the highest excitation density). The computed reexcitation is compared with the experimental initial excitation (defined as the product of the laser power density and the absorption coefficient at the laser wavelength), both in absolute units. Reabsorption is most intense at the beam center (this corresponds to effect (1) above—reflection at the epilayer surface) and then strongly decreases away from the beam. It is always orders of magnitude smaller than the initial excitation and therefore does not contribute to the PL signal that we measure.

It should be noted that the *total reexcitation* (integrated over the whole sample area) is actually not small—in this calculation, more than 10% of the emitted light eventually gets reabsorbed. However, this occurs over the whole area of the sample; therefore, the reexcitation density is very low, as shown above.

4. Multiple bounces

Despite the presence of antireflection coatings, a fraction of the PL is reflected at interfaces. Therefore, PL emitted off axis can travel laterally inside the sample and lead to a broadening or smearing out of the PL spot. We find that this effect is indeed significant at the highest laser

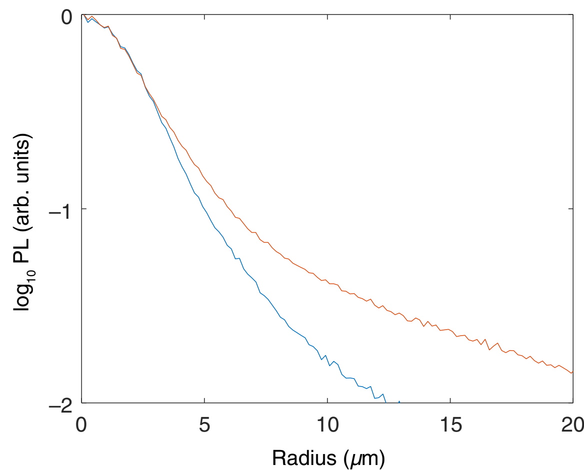

FIG. 8. The PL spot cross section at the maximum excitation density: blue, with an iris limiting the numerical aperture of the collection; red, without the iris.

density (where the PL spot is the sharpest), if no precautions are taken. Figure 8 compares two measurements at the highest laser intensity. In one, the numerical aperture of the collecting lens is not limited (leading to a collection $> 10^\circ$), whereas in the other a small iris (diameter 2 mm) placed in the collimated imaging path limits the collection to near-normal incidence. The former measurement shows an artificially broad tail caused by multiple-bounce PL. In the latter, off-axis PL is not collected and the intrinsic PL spot shape is resolved. In the rest of this paper, an iris is used to remove this artifact.

Note that the iris does not affect the results at a lower power density, where diffusion is stronger and the PL spot is broad, so that multiple-bounce PL does not lead to further broadening.

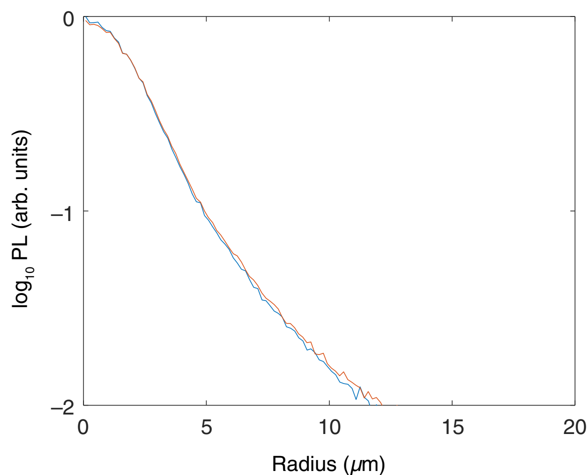

FIG. 9. The PL spot cross section at the maximum excitation density, with cw (blue line) and pulsed (red line) excitation. The two profiles are identical, showing that no thermal effects influence the results.

5. Nonlinear absorption

One might worry that two-photon absorption (2PA) could alter our measurements, leading to a nonlinear power dependence. However, 2PA is too low by orders of magnitude to contribute to PL. The 2PA coefficient in (In, Ga)N is on the order of $\beta \sim 10$ cm/GW. We are using a 70-mW cw laser diode; even at the peak laser intensity (say, with a 1-μm radius), the resulting 2PA absorption coefficient is thus approximately 0.02 cm^{-1}—to be compared with the linear absorption coefficient of approximately $10^4 - 10^5$ cm^{-1}.

6. Thermal effects

One might worry that lattice heating at high excitation could influence diffusion. However, the total absorbed laser power is small (approximately 2.5 mW at the highest density) and we expect it to be dissipated in the GaN substrate with its high thermal conductance. To verify this, we repeat a measurement at the maximum power, comparing the laser in cw mode and pulsed mode (100-ns pulses, 10-μs period, 1% duty factor). The PL profiles, shown in Fig. 9, are not affected by the duty factor.

[1] M. Mensi, R. Ivanov, T. K. Uzdavinys, K. M. Kelchner, S. Nakamura, S. P. DenBaars, J. S. Speck, and S. Marcinkevicius, Direct measurement of nanoscale lateral carrier diffusion: Toward scanning diffusion microscopy, ACS Photonics **5**, 528 (2018).

[2] J. Danhof, U. T. Schwarz, A. Kaneta, and Y. Kawakami, Time-of-flight measurements of charge carrier diffusion in $In_xGa_{1-x}N$/GaN quantum wells, Phys. Rev. B **84**, 035324 (2011).

[3] J. Danhof, H. Solowan, U. T. Schwarz, A. Kaneta, Y. Kawakami, D. Schiavon, T. Meyer, and M. Peter, Lateral charge carrier diffusion in InGaN quantum wells, Phys. Status Solidi (b) **249**, 480 (2012).

[4] A. Vertikov, I. Ozden, and A. V. Nurmikko, Diffusion and relaxation of excess carriers in InGaN quantum wells in localized versus extended states, J. Appl. Phys. **86**, 4697 (1999).

[5] R. Aleksiejunas, M. Sudzius, V. Gudelis, T. Malinauskas, K. Jarasiunas, Q. Fareed, R. Gaska, M. S. Shur, J. Zhang, and J. Yang, Carrier transport and recombination in InGaN/GaN heterostructures, studied by optical four-wave mixing technique, Phys. Status Solidi (c), 2686 (2003).

[6] A. David, N. G. Young, C. A. Hurni, and M. D. Craven, All-optical measurements of carrier dynamics in bulk-GaN LEDs: Beyond the *ABC* approximation, Appl. Phys. Lett. **110**, 253504 (2017).

[7] A. David, N. G. Young, C. A. Hurni, and M. D. Craven, Quantum Efficiency of III-Nitride Emitters: Evidence for Defect-Assisted Nonradiative Recombination and its Effect on the Green Gap, Phys. Rev. Appl. **11**, 031001 (2019).

[8] A. David, N. G. Young, and M. D. Craven, Many-Body Effects in Strongly-Disordered III-Nitride Quantum Wells:

Interplay between Carrier Localization and Coulomb Interaction, Phys. Rev. Appl. **12**, 044059 (2019).

[9] A. David, N. G. Young, C. Lund, and M. D. Craven, The physics of recombinations in III-nitride emitters, ECS J. Solid. State. Sci. Technol. **9**, 016021 (2019).

[10] A. David, N. Young, C. Lund, and M. Craven, Compensation between radiative and auger recombinations in III-nitrides: The scaling law of separated-wavefunction recombinations, Appl. Phys. Lett. **115**, 193502 (2019).

[11] A. David, C. A. Hurni, N. G. Young, and M. D. Craven, Field-assisted Shockley-Read-Hall recombinations in III-nitride quantum wells, Appl. Phys. Lett. **111**, 233501 (2017).

[12] S. J. Rosner, E. C. Carr, M. J. Ludowise, G. Girolami, and H. I. Erikson, Correlation of cathodoluminescence inhomogeneity with microstructural defects in epitaxial GaN grown by metalorganic chemical-vapor deposition, Appl. Phys. Lett. **70**, 420 (1997).

[13] A. Kaneta, M. Funato, and Y. Kawakami, Nanoscopic recombination processes in InGaN/GaN quantum wells emitting violet, blue, and green spectra, Phys. Rev. B **78**, 125317 (2008).

[14] T. Maeda, T. Narita, H. Ueda, M. Kanechika, T. Uesugi, T. Kachi, T. Kimoto, M. Horita, and J. Suda, Shockley-Read-Hall lifetime in homoepitaxial p-GaN extracted from recombination current in GaN p-n^+ junction diodes, Jpn. J. Appl. Phys. **58**, SCCB14 (2019).

[15] W. Liu, Ph.D. thesis, Ecole Polytechnique Federale de Lausanne, 2019.

[16] V. M. Kaganer, J. Lahnemann, C. Pfuller, K. K. Sabelfeld, A. E. Kireeva, and O. Brandt, Determination of the Carrier Diffusion Length in GaN from Cathodoluminescence Maps around Threading Dislocations: Fallacies and Opportunities, Phys. Rev. Appl. **12**, 054038 (2019).

[17] A. Fiore, M. Rossetti, B. Alloing, C. Paranthoen, J. X. Chen, L. Geelhaar, and H. Riechert, Carrier diffusion in low-dimensional semiconductors: A comparison of quantum wells, disordered quantum wells, and quantum dots, Phys. Rev. B **70**, 205311 (2004).

[18] S. F. Chichibu, A. Uedono, T. Onuma, B. A. Haskell, A. Chakraborty, T. Koyama, P. T. Fini, S. Keller, S. P. Denbaars, J. S. Speck, U. K. Mishra, S. Nakamura, S. Yamaguchi, S. Kamiyama, H. Amano, I. Akasaki, J. Han, and T. Sota, Origin of defect-insensitive emission probability in In-containing (Al, In, Ga)N alloy semiconductors, Nat. Mater. **5**, 810 (2006).

[19] R. Aleksiejunas, M. Sudzius, T. Malinauskas, J. Vaitkus, K. Jarasiunas, and S. Sakai, Determination of free carrier bipolar diffusion coefficient and surface recombination velocity of undoped GaN epilayers, Appl. Phys. Lett. **83**, 1157 (2003).

[20] S. Hammersley, D. Watson-Parris, P. Dawson, M. J. Godfrey, T. J. Badcock, M. J. Kappers, C. McAleese, R. A. Oliver, and C. J. Humphreys, The consequences of high injected carrier densities on carrier localization and efficiency droop in InGaN/GaN quantum well structures, J. Appl. Phys. **111**, 083512 (2012).

[21] G. Pozina, R. Ciechonski, Z. Bi, L. Samuelson, and B. Monemar, Dislocation related droop in InGaN/GaN light emitting diodes investigated via cathodoluminescence, Appl. Phys. Lett. **107**, 251106 (2015).

[22] W. Liu, R. Butte, A. Dussaigne, N. Grandjean, B. Deveaud, and G. Jacopin, Carrier-density-dependent recombination dynamics of excitons and electron-hole plasma in m-plane InGaN/GaN quantum wells, Phys. Rev. B **94**, 195411 (2016).

[23] A. Hangleiter, F. Hitzel, C. Netzel, D. Fuhrmann, U. Rossow, G. Ade, and P. Hinze, Suppression of Nonradiative Recombination by V-Shaped Pits in GaInN/GaN Quantum Wells Produces a Large Increase in the Light Emission Efficiency, Phys. Rev. Lett. **95**, 127402 (2005).

[24] C. Haller, J. F. Carlin, G. Jacopin, D. Martin, R. Butte, and N. Grandjean, Burying non-radiative defects in InGaN underlayer to increase InGaN/GaN quantum well efficiency, Appl. Phys. Lett. **111**, 262101 (2017).

[25] S. Watanabe, N. Yamada, M. Nagashima, Y. Ueki, C. Sasaki, Y. Yamada, T. Taguchi, K. Tadatomo, H. Okagawa, and H. Kudo, Internal quantum efficiency of highly-efficient $In_xGa_{1-x}N$-based near-ultraviolet light-emitting diodes, Appl. Phys. Lett. **83**, 4906 (2003).

[26] S. Karpov, ABC-model for interpretation of internal quantum efficiency and its droop in III-nitride LEDs: A review, Opt. Quantum Electron. **47**, 1293 (2015).

[27] B. Galler, P. Drechsel, R. Monnard, P. Rode, P. Stauss, S. Froehlich, W. Bergbauer, M. Binder, M. Sabathil, and B. Hahn, Influence of indium content and temperature on Auger-like recombination in InGaN quantum wells grown on (111) silicon substrates, Appl. Phys. Lett. **101**, 131111 (2012).

[28] F. Olivier, S. Tirano, L. Dupre, B. Aventurier, C. Largeron, and F. Templier, Influence of size-reduction on the performances of GaN-based micro-LEDs for display application, J. Lumin. **191**, 112 (2017).

[29] M. S. Wong, C. Lee, D. J. Myers, D. Hwang, J. A. Kearns, T. Li, J. S. Speck, S. Nakamura, and S. P. DenBaars, Size-independent peak efficiency of III-nitride micro-light-emitting-diodes using chemical treatment and sidewall passivation, Appl. Phys. Express **12**, 097004 (2019).